Vol. 22: 59–76, 2014
doi: 10.3354/ab00585

AQUATIC BIOLOGY
Aquat Biol

Published November 20

Contribution to the Theme Section 'Environmental forcing of aquatic primary productivity'

OPEN ACCESS CC BY

Effect of CO_2, nutrients and light on coastal plankton. III. Trophic cascade, size structure and composition

A. Reul[1,*], M. Muñoz[1], B. Bautista[1], P. J. Neale[2], C. Sobrino[3], J. M. Mercado[4], M. Segovia[1], S. Salles[4], G. Kulk[5], P. León[4], W. H. van de Poll[6], E. Pérez[1], A. Buma[5], J. M. Blanco[1]

[1]Universidad de Málaga, Andalucía Tech, Departamento de Ecología, Campus de Teatinos s/n, 29071 Málaga, Spain

[2]Smithsonian Environmental Research Center, Edgewater, Maryland 21037, USA

[3]Department of Ecology and Animal Biology, Faculty of Sciences, University of Vigo, Campus Lagoas-Marcosende s/n, 36310 Vigo, Spain

[4]Centro Oceanográfico de Málaga, Instituto Español de Oceanografía, Puerto Pesquero s/n, 29640 Fuengirola, Málaga, Spain

[5]Department of Ocean Ecosystems, Energy and Sustainability Research Institute Groningen, University of Groningen, Nijenborgh 7, 9747 AG Groningen, The Netherlands

[6]Department of Biological Oceanography, Royal Netherlands Institute for Sea Research (NIOZ), PO Box 59, 1790 AB, Den Burg, The Netherlands

ABSTRACT: We investigated the impacts of climate change-associated abiotic factors on the species composition and size structure of coastal phytoplankton communities. Surface coastal water collected off the coast of Málaga (Spain) was incubated outdoors during a 7 d microcosm experiment. The natural phytoplankton communities were exposed to high and low conditions of CO_2, nutrients and light. During the first 2 d, a positive response to increased CO_2 and nutrient concentration was observed in terms of abundance and chlorophyll in all size fractions (<2, 2 to 20, and >20 µm). After 2 d, a trophic cascade effect was observed within the phytoplankton communities for all treatments. The absence of mesozooplankton led to an increase in microzooplankton abundance, which coincided with a decrease in the abundance of phytoplankton <6 µm equivalent spherical diameter (ESD). At the same time, an increased concentration of larger phytoplankton was observed. Consequently, a diatom bloom dominated by *Leptocylindrus danicus* and *Chaetoceros* sp. developed, peaking on Day 5 in the high-light treatment and on Day 6 in the low-light treatment. The cascade effect was evident in both the smaller and the larger ranges of the size–abundance spectra (SAS). Although this trophic interaction occurred in all treatments in a similar way, there were still significant differences among treatments. Diatoms with cell sizes >20 µm ESD showed a positive response to the effects of increasing CO_2 and nutrient concentration. These results highlight the importance of trophic interactions other than abiotic factors such as CO_2 and nutrient availability in shaping the size structure of Mediterranean phytoplankton. More specifically, this work shows the importance of trophic cascade effects in scaling the plankton SAS and should be considered in both enclosure experiments and field measurements that deal with size distribution.

KEY WORDS: Microcosm · CO_2 · Nutrients · Phytoplankton · Composition · Size structure · Top-down · Trophic cascade

INTRODUCTION

Quantifying the efficiency of the ocean's biological pump, which removes CO_2 from surface waters and sequesters carbon into deep waters (Falkowski et al. 2000), is still one of the priorities in oceanographic science. The resulting decrease of CO_2 in surface waters promotes the absorption of CO_2 from the atmosphere (Sabine et al. 2004, Behrenfeld et al. 2006) and mitigates the effects of global warming. Further-

*Corresponding author: areul@uma.es

© The authors 2014. Open Access under Creative Commons by Attribution Licence. Use, distribution and reproduction are unrestricted. Authors and original publication must be credited.

Publisher: Inter-Research · www.int-res.com

more, one-third of the anthropogenic CO_2 produced since the industrial revolution has been absorbed by the oceans (Sabine et al. 2004). However, most of the anthropogenic CO_2 remains above the permanent thermocline and up to 30% remains in the upper 200 m of the water column (Sabine et al. 2004). This leads to the acidification of the euphotic layer (Feely et al. 2004, Sabine et al. 2004, Orr et al. 2005), which can affect physiological processes (Sobrino et al. 2008) and the composition of the phytoplankton community (Tortell et al. 2002). Apart from acidification, global warming may enhance stratification, which reduces nutrient availability in the euphotic layer by strengthening and shoaling of the thermocline (Boyd & Doney 2002, Polovina et al. 2008). Accordingly, phytoplankton may be exposed to increasing CO_2 concentrations, low nutrient concentrations and elevated irradiance in the surface waters of the open oceans. In contrast, high nutrient inputs, both from organic and inorganic origin, are expected for most of the coastal areas where changes in land use and hydrological cycles modify the amount and nature of continental inputs into the ocean (Duce et al. 2008).

Perturbation experiments with cultures in the laboratory (Hoffmann et al. 2008) or with natural assemblages in the field (Boyd et al. 2007, Hare et al. 2007, Feng et al. 2009, Riebesell et al. 2010) are suitable to explore environmental control on phytoplankton. However, the effect of increased CO_2 on primary production depends on the species (Tortell et al. 2002, 2008) and the synergistic effects of different environmental factors. Synergistic effects in particular imply major uncertainties about which phytoplankton species will either benefit or suffer from global climate change. Thus, realistic multivariate experimental studies are necessary in order to improve the predictions of changes in phytoplankton community compositions in the future (Boyd et al. 2010, Gao et al. 2012). Apart from abiotic factors, trophic interactions and size distribution of the organisms are key factors for channelling energy and biomass through the pelagic ecosystem (Hairston & Hairston 1993, Cury et al. 2003). On the other hand, future changes in the planktonic composition due to global climate change could also imply cascade effects (Stibor et al. 2004, Essington 2010), which could amplify the impact of community shifts of phytoplankton caused by abiotic factors.

While most studies involving phytoplankton are focused on primary production, metabolic rates, CO_2 incorporation and species composition, few studies address changes in size structure and trophic interactions. However, cell size plays a key role in channelling material and energy through the food web (microbial vs. classical food web) and in the effectiveness of the biological pump (Legendre & Le Fèvre 1989, Legendre et al. 1993). The present study aims to improve our understanding of the composition and size structure of coastal phytoplankton communities exposed to simultaneously changing environmental factors.

In order to investigate the combined effect of CO_2, nutrients and light on natural phytoplankton assemblages, a 7 d outdoor microcosm experiment was carried out in the framework of the 9th GAP workshop. The experimental setting and the physical, chemical and biological patterns are described in Neale et al. (2014, this Theme Section), metabolic rates are described in Mercado et al. (2014, this Theme Section), and phytoplankton physiological responses are described in Sobrino et al. (2014, this Theme Section). In the present study, flow cytometry, fluorospectrometry, flow cytometer and microscope (FlowCAM®, Fluid Imaging Technologies), microscopy and HPLC analysis were used to assess the composition, abundance and size structure of phytoplankton groups within the experimental communities. The results are discussed in the context of the complexities of interactions at the community level.

MATERIALS AND METHODS

Experimental set-up

The microcosm experiment was carried out in 24 low-density polyethylene UVR transparent 'cubitainers', each filled with 20 l of coastal seawater. Almost 900 l of surface (0 to 1 m) water was collected at 10:00 h on 15 September 2012 (Day –1) about 2 km off the coast of Málaga, and immediately transported in the dark. The seawater was screened through a 200 µm mesh as it was collected to remove mesozooplankton. Mesozooplankton are generally not well represented in microcosm volumes of 20 l, and their presence in the experiment would have caused uneven grazing effects among the microcosm replicates which would have obscured statistical comparisons of the results. After screening, the collected seawater for the experiment was mixed in a large container for homogeneity prior to taking initial samples (Day –1). The cubitainers were then filled and transported to the roof of the Spanish Institute of Oceanography site in Fuengirola (36.54° N, 4.60° W), where they were placed in large water baths. The next morning, just before the application of the treatments, Day 0 samples were taken from the cubitainers. The tempera-

ture of the water baths was maintained close to sea surface temperature at the sampling site (20 to 22°C) by a circulation system equipped with 3 Aqua-Medic-Titan-500 coolers, and continuously measured by HOBO Pendant UV temperature/light loggers. Each of the 3 factors considered in the experiment, carbon (C), light, (L), and nutrients (N), were applied in high (H) and low (L) conditions. Their combination led to a total of 8 treatments (Table 1), each with 3 replicates. Average pCO_2 in the HC and LC treatments corresponded to 1050 ± 70 and 453 ± 11 ppmv, respectively. HN corresponded to tanks fertilized on Day 0 with 3.0 µM NO_3^- and 0.2 µM PO_4^{3-}. On Day 2, another pulse of PO_4^{3-} was added in order to restore the initial ratio (see details in Neale et al. 2014). LN corresponded to natural nutrient availability in sampled water on Day −1 (0.54 µM NO_3^- and 0.14 µM PO_4^{3-}). Average mid-day photosynthetically active radiation (PAR) in the microcosms was 539 and 232 µmol m^{-2} s^{-1} for HL and LL treatments, respectively (Neale et al. 2014).

The experiment lasted 7 d in order to encompass a time period expected for acclimation to the experimental conditions (Sobrino et al. 2005, 2008, 2009). Sampling of the cubitainers was carried out between 09:00 and 09:30 h; the 8 treatments were sampled simultaneously by different persons while the replicates were sampled successively (A, B, C). All cubitainers were sampled daily for flow cytometry, nutrient and fluorospectrometer analysis, and on Days 0, 2, 4 and 6 for microscope and FlowCAM analysis. At the end of the experiment, samples were taken for variables requiring large volumes, such as HPLC. For more details of the experimental set-up, see Neale et al. (2014).

Flow cytometry

For the analysis of phytoplankton with cell sizes <15 µm equivalent spherical diameter (ESD), unfixed samples of each treatment were analyzed within 2 to 4 h after sampling using a FACScan flow cytometer. The acquisition time was 60 s (0.644 ml) and the following instrument settings were used: forward scatter (FSC) = E00, side scatter (SSC) = 271 mV, fluorescence 563 to 607 nm (Fl2) = 450 mV and fluorescence >650 nm (Fl3) = 300 mV. In order to detect only fluorescent particles, the threshold was set on the first channel of Fl3. Although FSC is more frequently used for size estimation by flow cytometry (Reul et al. 2002, Rodríguez et al. 2002), both FSC and SSC are related to size (Volkmer & Heinemann 2011) and have been used in oceanographic studies (Reul et al. 2002, Rodríguez et al. 1998). In this study, the SSC channel signal was calibrated for size conversion with living cultures before the start of the experiment, because the SSC calibration (r^2 = 0.989) showed a stronger relationship with cell size than the FSC calibration (r^2 = 0.909). To this end, 7 cultures with different sizes (Fig. 1a) were passed through the flow cytometer, and immediately afterwards, the cell size of 200 cells of the culture was measured by image analysis under an inverted microscope. The longest and shortest axes of each cell were measured and cell volume was calculated assuming spherical shapes. To avoid movement of the cells just before the measurements, a drop of non-acidic Lugol's iodine solution for microscopy was added, and cell sizes were measured immediately after fixation in order to avoid fixing effects (Ohman & Snyder 1991). When all measurements were completed, a linear regression was calculated between the SSC signal and the cell size of the cultures (Fig. 1a). Once acquired, the fluorescence and light scatter signals of each cell, phototrophic cell abundance and size distribution was determined with Attractors Software and saved as a gated FSC-file. Afterwards, size–abundance spectra (SAS) (see Blanco et al. 1994 for more details) were calculated automatically with custom software, where all cells were classified in octave-scaled size classes and the abundance in each class was presented against the geometrical mean of each size class in a $\log_{10}$ plot (Fig. 1b). After calculations of the SAS, the abundance and biovolume of cells of sizes <15 µm ESD was calculated as the sum of the abundance and the sum of the product of cell volume multiplied by the abundance in each size class.

Table 1. The 8 combinations of CO_2, nutrient and light treatments used in the microcosm experiment

Treatment			Abbreviation
High CO_2	High nutrient	High light	HC HN HL
High CO_2	Low nutrient	High light	HC LN HL
High CO_2	High nutrient	Low light	HC HN LL
High CO_2	Low nutrient	Low light	HC LN LL
Low CO_2	High nutrient	High light	LC HN HL
Low CO_2	Low nutrient	High light	LC LN HL
Low CO_2	High nutrient	Low light	LC HN LL
Low CO_2	Low nutrient	Low light	LC LN LL

FlowCAM

In order to count and measure the phytoplankton with cell sizes between 15 and 100 µm ESD, 30 ml of each experimental treatment was filtered through a

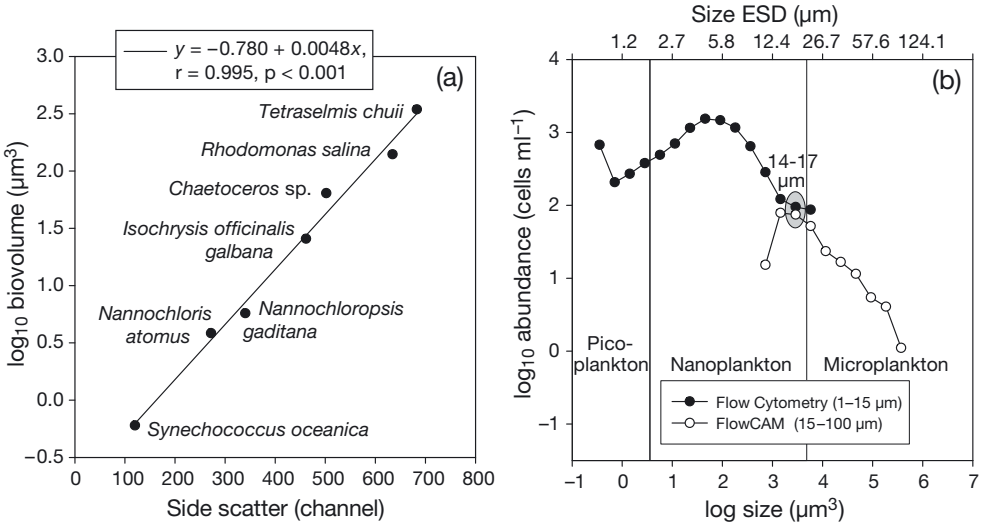

Fig. 1. (a) Calibration of flow cytometer side scatter (SSC) channel, (b) example of flow cytometry and FlowCAM combined size–abundance spectra. ESD: equivalent spherical diameter

100 µm mesh and immediately passed through the FlowCAM equipped with a 100 µm flow cell and a 100-fold magnification (10× objective). In the fluorescence triggered mode, digital images were only taken of particles with red fluorescence emission above a threshold of 400 (relative fluorescence intensity). In all samples, flow rates were adjusted to guarantee that no more than 1 particle appeared in each frame. The imaged volume of the samples that passed through the flow cell was 36%, thus all fluorescence particles in 10.84 ml of each sample were imaged (analyzed). The analysis of each sample took about 30 min. Once digital images and statistical information of all fluorescence particles were acquired, each sample was reprocessed in order to eliminate particles that did not correspond to phytoplankton. Then, the abundance and cell volume (assuming ESD, μm^3) of each particle was used to obtain the SAS, classifying the cells within an octave scale. Finally, the calculated SAS (15 to 100 µm) were combined with the flow cytometry SAS (0.7 to 15 µm) in order to construct SAS between 0.7 and 100 µm ESD (Fig. 1b). Further details concerning FlowCAM abundance and size distribution measurements are provided in Álvarez et al. (2012, 2014)

Fluorospectrometer

In order to measure the composition and size distribution of phytoplankton, 20 ml of each sample was analysed by a fluorospectrometer (FluoroProbe, BBE Moldaenke) equipped with a workstation, which permits the analysis of discrete samples.

The fluorospectrometer discriminated between the main phytoplanktonic groups (i.e. diatoms and dinoflagellates, blue-green algae, green algae and cryptophytes) based on the relative fluorescence intensity of chlorophyll *a* (chl *a*) at 680 nm, following sequential light excitation by 5 light-emitting diodes (LEDs) emitting at 450, 525, 570, 590 and 610 nm (Beutler et al. 2002, Leboulanger et al. 2011). Depending on the accessory pigments, a set of characteristic fingerprints can be detected and used for recognition of these groups in natural phytoplankton samples. Finally, the relative amount of each algal class present in the sample was calculated and expressed in terms of the equivalent amount of chl *a* ($\mu g\ l^{-1}$). After the fluorescence measurement, each sample was screened and measured sequentially through 20 and 2 µm meshes, allowing the calculation of 3 size-fractions: picophytoplankton (<2 µm), nanophytoplankton (2 to 20 µm), and microphytoplankton (>20 µm).

The fluorescence in the picophytoplankton size fraction was very low (see Fig. 5b) and algal classification could not be resolved fluorometrically. Thus, according to the upper size limit, this fraction is referred to picophytoplankton chl *a* without differentiation between varying phytoplankton groups.

Microscope analysis

Selected samples of each treatment were analysed by microscope every second sampling day. Samples were collected in 120 ml opal glass bottles and fixed with acidic Lugol's solution (3% final conc.) to be analyzed using the Utermöhl technique (Utermöhl 1958). To this end, a volume of 25 to 50 ml was settled in a chamber for 24 h and analyzed on a Nikon Eclipse TS100 optical inverted microscope. A sufficient number of fields (at least 2 transects) were

counted at 200× magnification until at least 100 individuals of the most abundant species or genera were registered (Ros & Miracle 1984). Small flagellates were counted using 600× magnification. Furthermore, the bottom of the chamber was scanned at 40× magnification in order to count the larger cells. This procedure was additionally used to determine microzooplankton (ciliate) abundance in all samples analysed. The smallest size limit for microscopic enumeration was established at 5 µm. Where possible, phytoplankton organisms were identified at the genus or species level following species nomenclature of Tomas (1997). Due to time constraints, microscopic analysis (phytoplankton taxonomy and ciliate abundance) was carried out for only 1 replicate of each treatment.

HPLC

Samples for HPLC analysis were obtained from all treatments on Day 6, filtered on 47 mm GF/F, snap frozen in liquid nitrogen, stored at −80°C and analyzed according to Hooker et al. (2009). After analysis, phytoplankton taxonomic composition was determined using CHEMTAX (Mackey et al. 1996). In short, 13 pigments (chl *a*, dv chl *a*, chl *b*, chl *c2*, chl *c3*, peridinin, fucoxanthin, 19-butanoyloxyfucoxanthin, 19-hexanoyloxyfucoxanthin, neoxanthin, prasinoxanthin, alloxanthin and zeaxanthin) were used to distinguish 8 taxonomic groups (*Synechococcus, Prochlorococcus*, haptophytes, diatoms, dinoflagellates, cryptophytes, prasinophytes and pelagophytes). Taxonomic composition was calculated using initial pigment ratios for high-light acclimated phytoplankton according to van de Poll et al. (2013). Contributions of the identified taxonomic groups to total chl *a* were calculated.

Statistics

To discriminate among the effect of CO_2, nutrients and light, a repeated-measures ANOVA was carried out on size fractionated diatoms and green algal chl *a* concentrations (see Table 2). The relationships between variables presented in Figs. 1a, 2a,b, 6, 7b & 8 (see 'Results' section) were calculated by linear regression analysis. Prior to statistical analysis, all data were tested for normality (Kolmogorov-Smirnov) and constant variance (Spearman rank correlation between the absolute values of the residuals and the observed value of the dependent variable).

RESULTS

Fluorospectrometer calibration

The applied fluorospectrometer fingerprint method grouped diatoms and dinoflagellates in the same group ('diatoms & dinoflagellates'), but the microscope analysis showed a low contribution of dinoflagellates to the total phytoplankton abundance >5 µm during the whole experiment. The relative numerical contribution of dinoflagellates was less than 11% at Day −1 and less than 6% between Days 2 and 6. In addition, the initial and final composition of the phytoplankton community confirmed that diatoms dominated the phytoplankton assemblages in the >15 µm size range (see Appendix). Therefore, in this study we refer to diatoms as only the fluorospectrometer chl *a* concentration corresponding to the diatom & dinoflagellate fingerprint. In order to verify the results of the fluorospectrometer, total and diatom-related chl *a* concentration were compared with independent chl *a* measurements.

The comparison of spectrophotometrically-derived chl *a* and chl *a* concentrations after acetone extraction, as well as the comparison of total-chl *a* and diatom-chl *a* concentrations estimated from fluorospectrometer with HPLC measurements showed consistent results (Fig. 2a). This demonstrated that the fluorospectrometer provided comparable chl *a* and phytoplankton composition data. This was additionally confirmed by the significant positive relationship between diatom abundance from microscope counts and fluorospectrometer-determined diatom chl *a* concentration (Fig. 2b).

Abundance, biovolume and size structure of cells <15 µm

Although HN treatments showed higher abundance and biovolume values of phytoplankton with cell sizes <15 µm than LN treatments on the first sampling day (Day 2), an important temporal pattern was observed in all treatments (Fig. 3). Based on flow cytometry, phytoplankton abundance <15 µm did not vary between the beginning of the experiment and Day 2, but decreased between Days 2 and 3 by a factor of 4.5 (from 45 000 cells ml^{-1} to less than 10 000 cells ml^{-1}; Fig. 3a). In contrast, biovolume increased by a factor of 4.3 from the initial value (1.3×10^6 μm^3 ml^{-1} on Days −1 and 0) to Day 2 (4 to 6×10^6 μm^3 ml^{-1}) and did not vary between Days 2 and 3 (Fig. 3b). On Day 4, biovolume decreased by a factor of 2 (from 6 ×

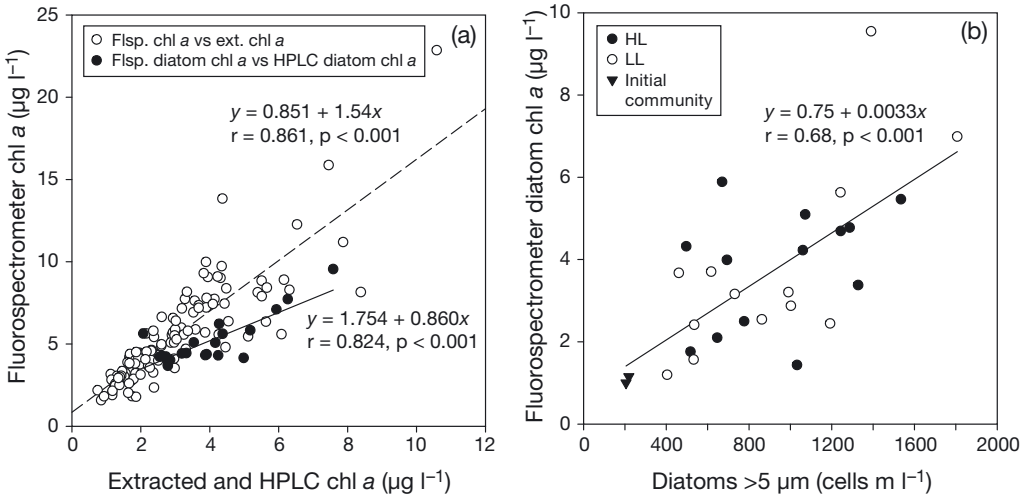

Fig. 2. (a) Fluorospectrometer (Flsp.) chl *a* concentrations versus extracted (ext.) total chl *a* concentrations and HPLC-derived chl *a* concentrations of diatoms; (b) relationship between diatom abundance (>5 µm) counted under the microscope and diatom chl *a* concentrations of the fluorospectrometer

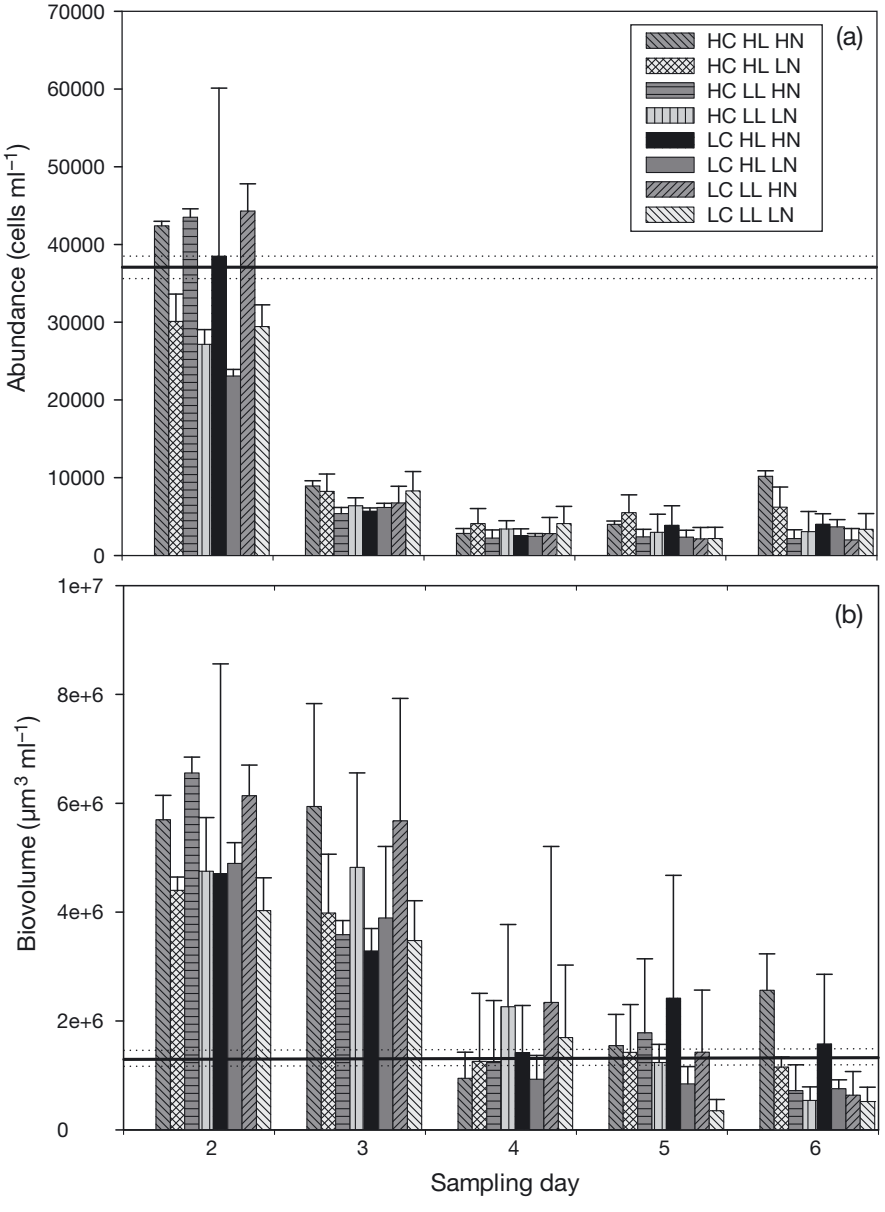

Fig. 3. (a) Abundance of phytoplankton with cell sizes <15 µm and (b) biovolume of phytoplankton with cell sizes <15 µm as measured by flow cytometry (mean ± SD). Horizontal line shows the mean of the initial community (mean Days −1 and 0) and the dotted lines indicate the corresponding SD

10^6 at Day 3 to $<3 \times 10^6$ µm^3 ml^{-1} at Day 4). Both (1) the similar abundance and increasing biovolume between Days 0 and 2 and (2) the decreasing abundance and similar biovolume between Days 2 and 3 indicated changes in the size structure of phytoplankton <15 µm as depicted in Fig. 4.

In comparison to the initial phytoplankton community (SAS of Days −1 and 0), the SAS at Day 2 can be divided into 2 fractions: (1) cells <6 µm (referred in this article to as ultraphytoplankton), which showed a decreased SAS between Days 0 and 2, and (2) cells with cell sizes >6 µm, which showed an increased SAS between Days 0 and 2 (Fig. 4). The increased abundance of cells with cell sizes >6 µm ESD corresponded to the observed general increase of biovolume on Day 2 in all treatments. On Day 3, the biovolume remained similar to that of Day 2, but abundance decreased to 10 000 cells ml^{-1} (Fig. 3). This pattern can be explained by the decreasing abundance of cells <6 µm on Day 3, while the abundance of cells >6 µm showed similar abundance compared with Day 2 (Fig. 4). Therefore, biovolume was less affected by the change in phytoplankton size structure than abundance (Fig. 3). Finally, on Day 4, the mean SAS showed the lowest abundances of cells <6 µm ESD, and cells with size >6 µm ESD decreased but still remained above the initial values. After the described initial changes between Days 0 and 4, the SAS (<15 µm ESD) remained similar until Day 6.

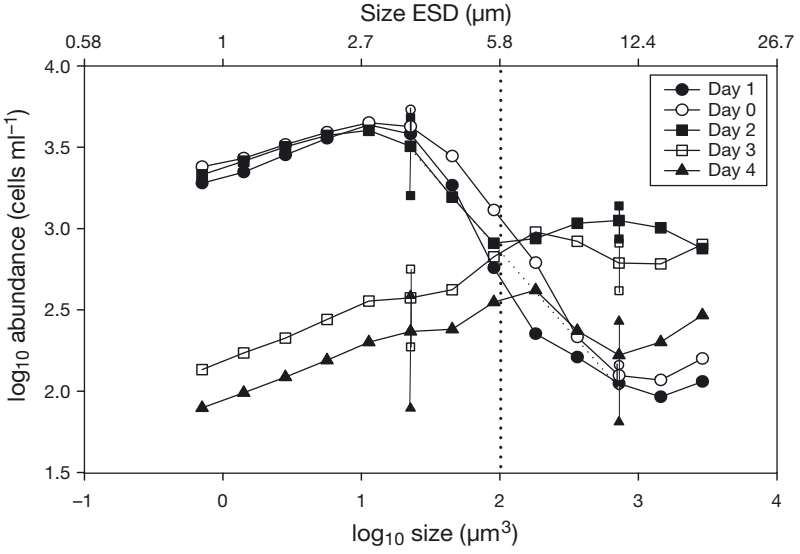

Fig. 4. Mean size–abundance spectra (SAS) of phytoplankton with cell sizes of 0.7 to 15 µm ESD on Day −1, 0, 2, 3, and 4. The vertical dotted line indicates the division of the SAS in cells with cell sizes <6 µm ESD and >6 µm ESD, which coincide approximately with the upper limit of micrograzing prey size. In order to show the variability among the SAS of the same day, vertical bars indicating SD of the mean SAS are shown at size classes with a geometric mean of 3.5 µm ESD ($\log_{10} = 1.346$) and 11.1 µm ESD ($\log_{10} = 2.86$)

Size-fractionated composition

The size fractionated fluorospectrometer measurements (fluoroprobe) provided insight into the composition and size structure of the whole phytoplankton community. The chl *a* concentration of the most important groups in terms of fluorescence intensity detectable with the applied fingerprint method—green algae and diatoms (Fig. 5a)—increased from the initial values (diatoms: 1 µg chl *a* l^{-1}; green algae: 0.3 µg chl *a* l^{-1}) up to 8 times for diatoms (8.5 µg chl *a* l^{-1}, treatment HC HN LL) and up to 10 times for green algae (3.1 µg chl *a* l^{-1}, treatment LC LN HL). For diatoms, the LN treatments always showed the lowest chl *a* concentration, especially in the LL treatments. In both phytoplankton groups, highest chl *a* concentrations were observed on Day 5, with the maximum chl *a* concentration increasing between Days 3 and 5 for diatoms and between Days 4 and 5 for green algae. The chl *a* concentration of both phytoplankton groups decreased at Day 6, except in the LL treatments (LC LN LL, HC LN LL and HC HN LL).

The analysis of different size fractions showed an initial value of picoplankton of 0.64 µg chl *a* l^{-1}, which increased in the HN treatments and decreased in the LN treatments at Day 2 (Fig. 5b). After the initial response of picophytoplankton to the nutrient treatment, the picoplankton chl *a* concentration decreased in all treatments between Days 2 and 3, reaching minimum values on Day 4, similar to ultraphytoplankton abundance and biovolume (Fig. 3).

The nanophytoplankton size fraction (2 to 20 µm) (Fig. 5c,d) showed increases in green algae and diatom chl *a* concentrations between Days 0 and 5. Diatoms especially showed a significantly higher chl *a* concentration in the HN treatments compared with the LN treatments (Fig. 5d, Table 2a). The nanophytoplankton fraction reached highest diatom chl *a* concentration on Day 5 and decreased on Day 6.

The microphytoplankton size fraction (>20 µm) also increased from the initial diatom chl *a* concentration (0.24 ± 0.12 µg chl *a* l^{-1}) up to Day 5 in all treatments. At Day 6, the chl *a* concentration decreased in the HL treatment and increased in the LL treatments, except for the LC LL HN treatment, suggesting that these treatments were light-limited

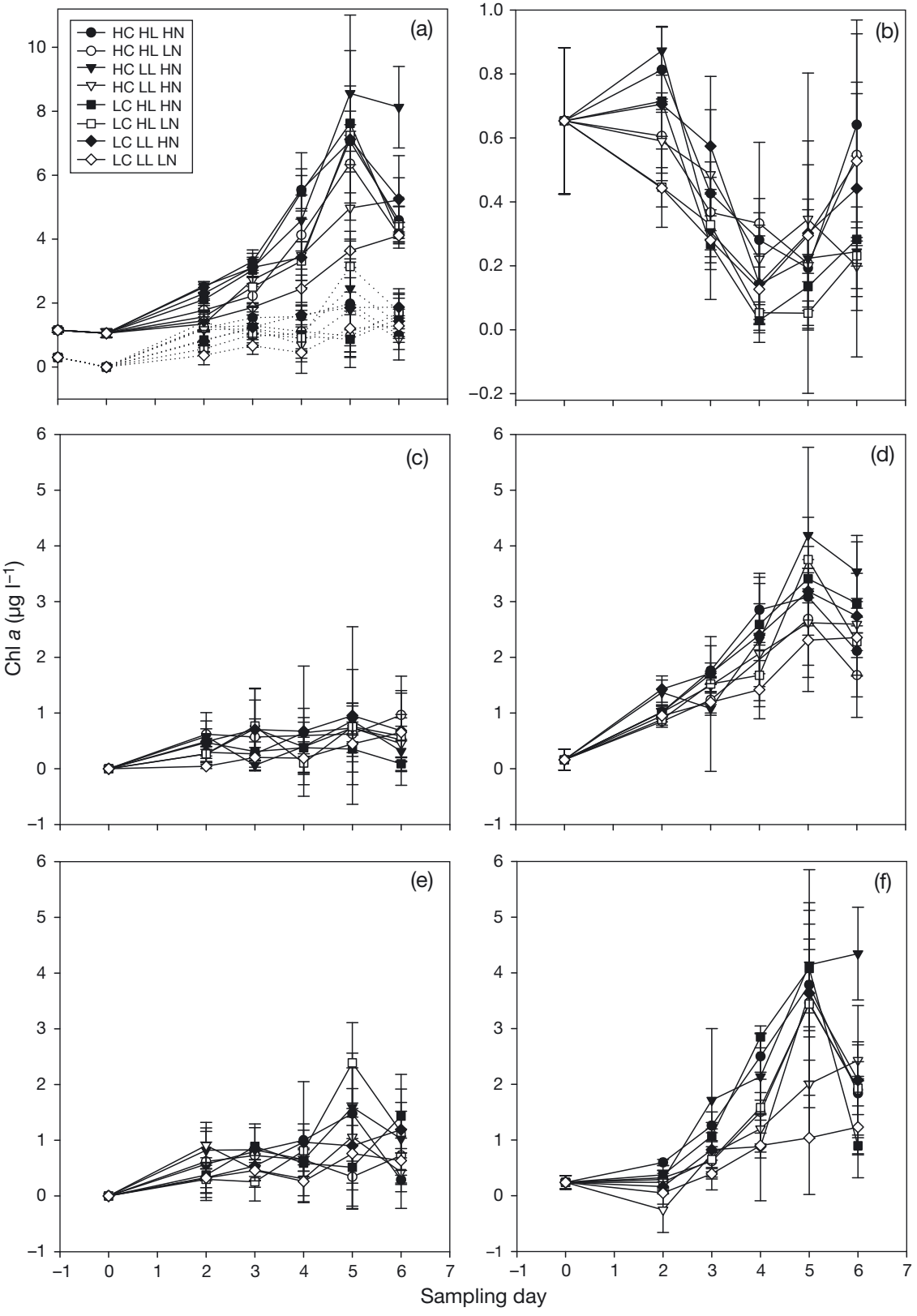

Fig. 5. Mean ± SD phytoplankton size fractions and composition of fluorescence-derived chl *a* concentrations (fluorospectrometer). (a) Total diatoms (solid lines) and green algae (dotted lines), (b) picoplankton, (c) green algae 2 to 20 µm, (d) diatoms 2 to 20 µm, (e) green algae >20 µm, and (f) diatoms >20 µm

Table 2. Repeated-measures ANOVA testing the main effects of each factor on the average of the 5 time intervals. Independent factors are CO_2, nutrient and light treatments and dependent variables are the 2 diatom and green algae size fractions (>20 µm, 2 to 20 µm) and picophytoplankton (<2 µm). *p < 0.05

Source of variation	df	Diatoms >20 µm			Diatoms 2–20 µm			Picophytoplankton <2 µm			Green algae >20 µm			Green algae 2–20 µm		
		MS	*F*	p	MS	*F*	p	MS	*F*	p	MS	*F*	p	MS	*F*	p
Intercept	1	173.888	325.360	<0.001*	525.732	732.34	<0.001*	16.228	164.505	<0.001*	68.303	136.829	<0.001*	31.279	38.376	<0.001*
CO_2 (C)	1	3.435	6.428	0.022*	0.039	0.054	0.819	0.266	2.699	0.120	<0.001	0.001	0.982	0.350	0.429	0.522
Nutrient (N)	1	4.981	9.320	0.008*	6.365	8.867	0.009*	0.133	1.349	0.263	0.693	1.389	0.256	0.010	0.012	0.914
Light (L)	1	0.115	0.216	0.648	0.003	0.005	0.945	0.037	0.373	0.550	0.124	0.249	0.625	0.042	0.052	0.823
C × N	1	4.003	7.489	0.015*	0.012	0.017	0.898	0.010	0.100	0.756	0.390	0.782	0.390	0.247	0.303	0.590
C × L	1	4.102	7.675	0.014*	1.472	2.051	0.171	0.252	2.554	0.130	0.857	1.718	0.209	0.537	0.658	0.429
N × L	1	1.631	3.051	0.100	0.534	0.744	0.401	<0.001	<0.001	0.986	0.884	1.771	0.202	0.619	0.759	0.396
C × N × L	1	0.021	0.039	0.847	0.034	0.047	0.831	0.005	0.054	0.819	0.225	0.452	0.511	0.590	0.724	0.407
Error	16	0.534			0.718			0.099			0.499			0.815		

Table 3. Repeated-measures ANOVA results indicating significance of factor (C = CO_2, N = nutrients; L = light) interactions with time (T). *p < 0.05 according to Wilks' lambda, using the Greenhouse-Geisser correction when the assumption of sphericity was not met; ns = not significant. The table shows only interactions that were significant in at least one of the analysed size fractions. The combinations or size fractions not included in the table were not significant

Source of variation	Pico-plankton	Green algae >20 µm	Diatoms >20 µm
T × C	ns	ns	*
T × N	*	ns	ns
T × L	ns	ns	*
T × C × L	*	ns	*
T × C × N	ns	*	ns

and that succession in LL treatments was slower than in HL treatments.

The statistical analysis of the results revealed that diatoms in the nano- and microphytoplankton size range responded positively to nutrient enrichment (Fig. 5d,f, Table 2, $p < 0.01$) and, in the case of diatoms >20 µm, to variations in CO_2 concentration (Table 2, $p < 0.05$). Light had no significant effect on diatom chl *a* concentration during the experiment. For diatoms with cell sizes >20 µm, the interaction between C × N and C × L was significant (Table 2, $p < 0.05$). In contrast to diatoms, picophytoplankton and green algae showed no significant response to the treatments. Time also significantly affected the results ($p < 0.001$) in all groups and size fractions, supporting the described time evolution during the experiment. The significant interactions with time are shown in Table 3. Picoplankton showed significant interactions for T × N and T × C × L. No interaction for the 2 to 20 µm fractions were observed. Green algae >20 µm showed significant interaction for T × C × N and diatoms >20 µm showed significant interactions for T × C, T × L and T × C × L.

Microscope analysis

Phytoplankton

The fluorospectrometer measurements showed a considerable diatom bloom in all treatments, especially in the microphytoplankton size fraction. Five diatom genera were identified by microscopy (*Leptocylindrus danicus, Chaetoceros* sp., *Guinardia striata, Nitzschia longissima*, and *Pseudo-nitzschia* sp.). These groups all increased significantly with in-

creasing total diatom abundance ($p < 0.05$, Fig. 6a), except for *N. longissima. L. danicus* and *Chaetoceros* sp. were the most important groups from Day −1 (52 and 12%, respectively) to Day 6 (51 ± 13 and 28 ± 14%, respectively). Mean relative contribution of both diatom species during the whole experiment was 50 ± 10% for *L. danicus* and 27 ± 10% for *Chaetoceros* sp.

Ciliates

Ciliate abundance increased in all treatments between Days 0 and 4 (Fig.7a). Furthermore, a negative relationship between ciliate abundance and picophytoplankton ($p < 0.05$), as well as between ciliate abundance and ultraphytoplankton ($p < 0.05$) abundance was found (Fig. 7b).

Prokaryotic picophytoplankton

Different relationships were observed between total diatom chl *a* and *Synechococcus* and *Prochlorococcus* abundance. *Synechococcus* abundance decreased exponentially from initial values (around 40 000 to 60 000 cells ml^{-1}) to abundances around 100 cells ml^{-1} (treatment HC HN LL) as diatom chl *a* concentration increased (Fig. 8). In contrast, *Prochlorococcus* did not show any significant relationship with diatom chl *a* concentrations, but abundances diminished from 9000 ± 1615 cells ml^{-1} on Day −1 to 2977 ± 1897 cells ml^{-1} on Day 0, and dropped to around 1000 cells ml^{-1} during the rest of the experiment.

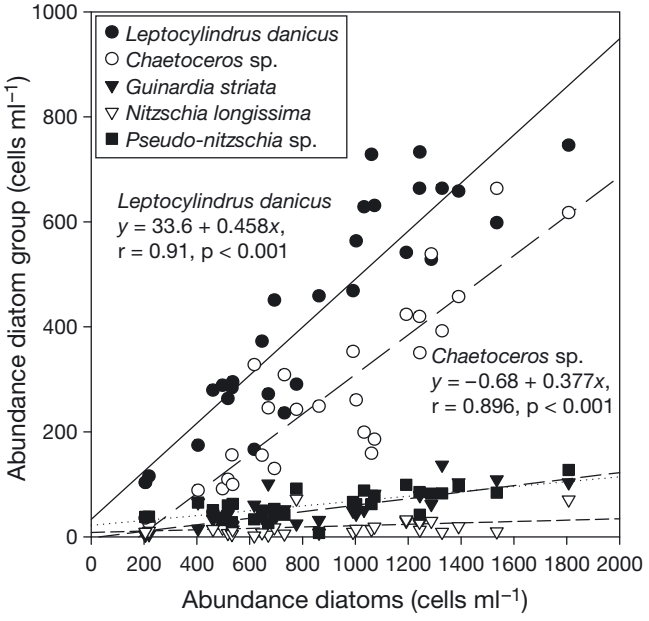

Fig. 6. Relationship between total diatom abundance and abundance of the 5 different diatom taxa which represented 94.5 ± 3.2% of total diatom abundance during the experiment

Size structure and phytoplankton composition at the end of the experiment

The phytoplankton community exhibited the largest differences among the 8 treatments on Day 5. However, the experiment lasted until Day 6, and due to

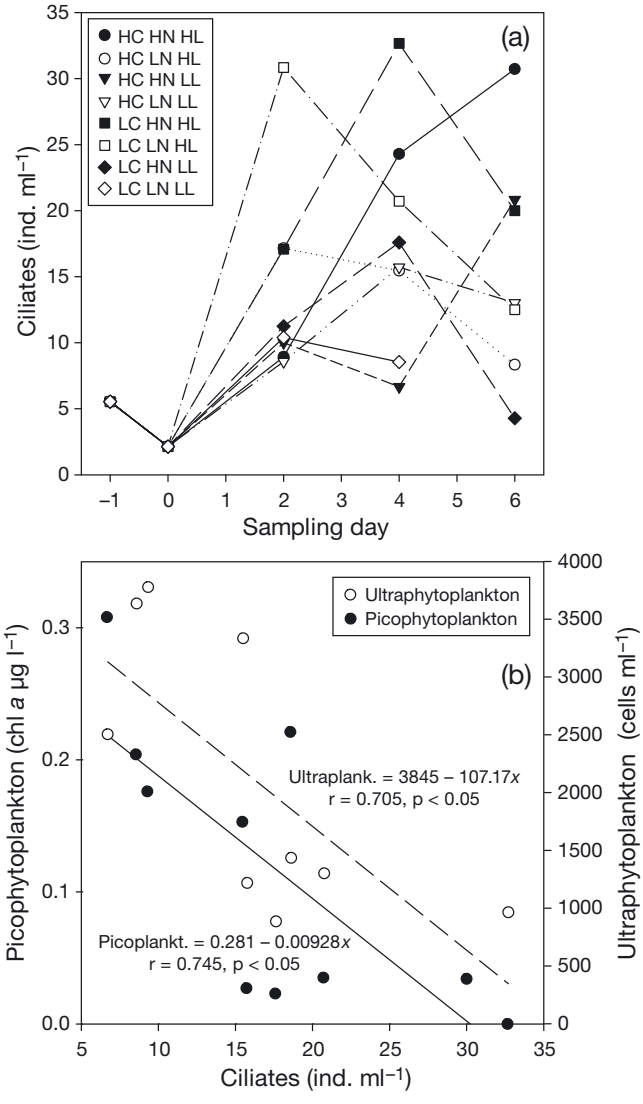

Fig. 7. (a) Time evolution of ciliate abundance in one replicate of each treatment during the experiment, (b) relationship between ciliate abundance, picophytoplankton (<2 µm) chl *a* concentration (µg l^{-1}) and ultraphytoplankton (cells <6 µm ESD) abundance (cells ml^{-1}) at Day 4

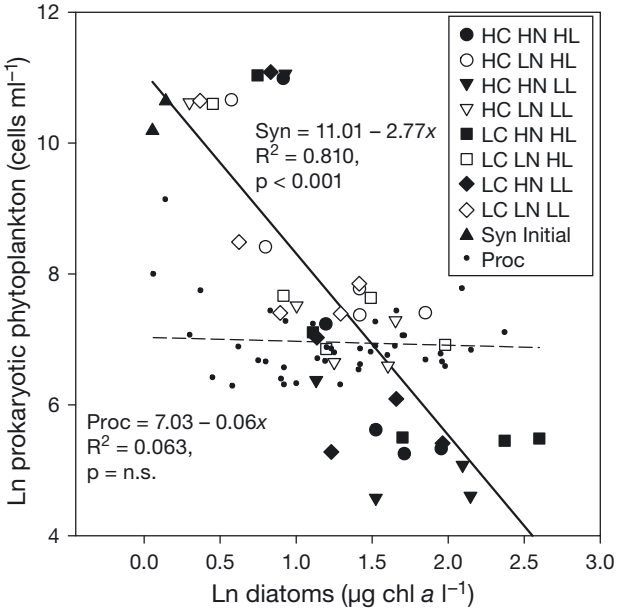

Fig. 8. Abundance of *Synechococcus* sp. and *Prochlorococcus* sp. as a function of diatom chl *a* (µg chl *a* l^{-1}) for all replicates during the experiment. Linear adjustments are shown for *Synechococcus* (Syn, continuous line) and *Prochlorococcus* (Proc, dashed line)

the limited water volume, several analyses were only carried out on even experimental days. Thus, complete SAS analysis was only available at Day 6 and not Day 5.

At Day 6 the SAS showed a dome-like pattern with highest abundance at around 6 µm ESD ($\log_{10}$ = 2.05, Fig. 9a). This distribution does not fit with a linear adjustment, which would allow the comparison of the slope and intercept using ANCOVA. Furthermore, the SAS on Day 6 were temporally decoupled from the starting SAS on Days –1 and 0. Therefore, we decided to compare the SAS of each sample with the mean SAS of all samples at Day 6 (Fig. 9a, grey line). To this end, we calculated the difference in terms of abundance and biovolume in each size class with

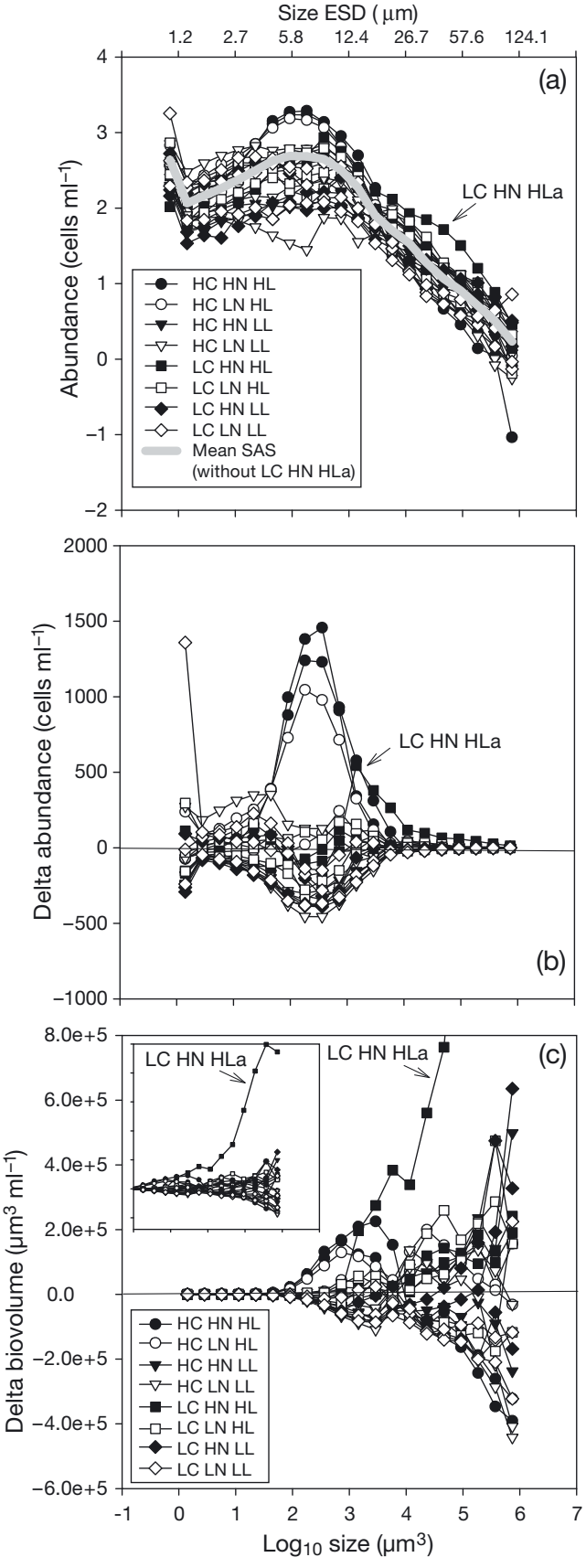

Fig. 9. (a) Complete size–abundance spectra (SAS) from 0.7 to 100 µm ESD of all treatments and mean SAS (grey line) at Day 6; (b) difference in the abundance of each size class of each SAS with respect to the abundance in each size class of the mean SAS; and (c) difference in the biovolume in each size class of each SAS with respect to the biovolume in each size class of the mean SAS. The LC HN HLa SAS corresponds to an unusually high phytoplankton bloom observed in replicate a of the LC HN HL treatment and (a) was not included in the mean SAS calculation, (b) shows the highest abundance between 12 and 15 µm ESD and (c) the highest delta biovolume >12 µm ESD

respect to the mean SAS at Day 6 (Fig. 9b and c, respectively). In terms of abundance, the SAS showed marked differences in the 6 to 12 µm ESD size fraction in 3 replicates of different experimental treatments (2 replicates of the HC HN HL treatment and 1 replicate of the HC LN HL treatment). In addition, one of the replicates of the LC HN HL treatment (denoted by LC HN HLa in Fig. 9b) showed a peak of cells in the 12 to 26 µm size fraction. Moreover, the delta abundance size distribution showed different patterns between the 3 replicates of each treatment (Fig. 9b). In terms of biovolume, the greatest variability among the SAS was observed in the size classes >6 µm (Fig. 9c). A marked difference in SAS was observed in one of the replicates from the LC HN HL (LC HN HLa) treatment, which showed a conspicuous diatom bloom that affected the biovolume. This SAS was not considered in the mean SAS calculation (Fig. 9a). However, a classification of the SAS according to delta biovolume was also not possible. It seems that the size structure of each community diverged as time progressed, and no common patterns among the SAS of the same treatments were observed at the end of the experiment.

Pigment signatures at the end of the experiment

In order to distinguish more phytoplankton groups in terms of pigment signatures, HPLC analysis was carried out on Day 6. The most important taxonomic groups detected by HPLC measurements at Day 6 were diatoms > dinoflagellates > haptophytes, while the remaining 5 identified classes (cryptophytes, chrysophytes and pelagophytes, *Synechococus* and *Prochlorococcus*) showed low values and almost no differences among the treatments (data not shown). In fact, a statistical difference ($p < 0.05$) was only found for the diatom concentrations, where the HC HN LL treatment showed significantly higher diatom concentration (6.60 µg l^{-1}) than the other treatments.

DISCUSSION

Cascade effects in the enclosed community

The experimental setup comprised the whole (autotrophic and heterotrophic) community that can pass through a <200 µm pore mesh. The changes in the size structure showed increasing abundances of cells >6 µm ESD and decreasing abundance of cells <6 µm ESD in all treatments. Since this pattern was independent of the experimental treatment, we suggest this to be due to cascade effects caused by the removal of mesozooplankton. The increasing abundance of cells of sizes >6 µm can be explained by alleviation of top-down control, as the most important grazers in this size range, cladocerans and copepods (Bautista & Harris 1992, Liu et al. 2005, Souza et al. 2005, Mercado et al. 2007) were removed at the beginning of the experiment. Furthermore, mesozooplankton also prey on microzooplankton (Calbet & Landry 1999, Calbet et al. 2012). The proportion of microzooplankton in the copepod diet is highly variable (Halvorsen et al. 2001) and depends mainly on the phytoplankton and zooplankton size structure. The *in situ* conditions of our experiment (chl *a* concentrations around 1 µg l^{-1}) suggest that microzooplankton was top-down controlled before the removal of the mesozooplankton (Fessenden & Cowles 1994, Ohman & Runge 1994). Thus, our interpretation is that: (1) In the natural environment, mesozooplankton directly control phytoplankton >6 µm and microzooplankton, releasing picophytoplankton from the top-down control of microzooplankton, and (2) by excluding mesozooplankton at the beginning of the experiment, both the phytoplankton >6 µm and microzooplankton responded to the lack of top-down control. This resulted in an increased abundance of cells with sizes >6 µm (Day 2), and a decrease in ultraphytoplankton abundance (Day 3) due to the increased grazing capacity of the recovered microzooplankton (ciliates).

Concerning cascade effects of mesozooplankton, Schlüter (1998) described high variability in growth and grazing rates, estimated by a dilution technique on 1 l pre-screened (200 µm) subsamples during a mesocosm (6000 l) experiment. Because this variability was not reflected in the biomass of the phytoplankton groups in the mesocosm, it was concluded that processes such as sedimentation and grazing by mesozooplankton are important loss processes that are not considered in dilution experiments or in any microphytoplankton enclosure experiment. Both processes might also affect our microcosm experiment. In fact, the importance of the trophic cascade in grazing (dilution) experiments is approached by different models (Calbet & Saiz 2013) and microcosm experiments (Modigh & Franzè 2009). In field measurements, the importance of mesozooplankton top-down effects on food web structure and vertical carbon transport was suggested by Hernández-León (2009). Recently, Schmoker et al. (2013) reviewed microplankton grazing data on a global scale and com-

pared them with the mesozooplankton grazing data of Calbet (2001). The global phytoplankton consumption rate of microzooplankton was about 62.4% of total primary production, 5 times higher than mesozooplankton grazing rates on phytoplankton (Schmoker et al. 2013).

Phytoplankton blooms are traditionally explained by bottom-up control, either due to external, internal or recycled-nutrient pools (Sun et al. 2013). Other approaches, such as the 'loophole' theory (Irigoien et al. 2005), include the top-down control of microzooplankton. According to the 'loophole' theory, the blooms are also initiated by the lack of microzooplankton top-down control. However, microzooplankton in turn are top-down controlled by mesozooplankton (Sommer et al. 2004). Consequently, although mesozooplankton are not the main consumers of primary production (Schmoker et al. 2013), they play a key role in structuring the planktonic community <200 µm through cascade effects. Intense upwelling processes, apart from nutrient input, may disrupt trophic coupling at the mesozooplankton level (Slaughter et al. 2006). Therefore, microphytoplankton proliferation during upwelling might be due to synergistic effects of both (1) favorable bottom-up conditions and (2) the relaxation of top-down control. Furthermore, faster intrinsic nutrient uptake and growth rate also provides an advantage to diatoms (Malone 1980).

Size structure

Size scaling of phytoplankton through size-dependent growth rates (Sarthou et al. 2005), nutrient quotas (Malone 1980) and light (Finkel 2001) are factors that potentially shape the size structure of the community based on bottom-up control (Irwin et al. 2006). However, our enclosure experiment showed that predator–prey relationships and cascade effects might be more important for scaling the plankton SAS than previously thought. The increasing microphytoplankton diatom fraction suggests that the absence of top-down control of microphytoplankton in the enclosures was the main driving force for the microphytoplankton bloom. It is worth noting that the absence of mesozooplankton affected both extremes of the SAS. Picophytoplankton decreased by increasing top-down control by microzooplankton, and microphytoplankton increased due to the lack in top-down control by mesozooplankton. The observation that the larger cell size fraction of the SAS diverged among the microcosm as time progressed indicates that the enclosed communities still present a very complex system. Such systems are very sensitive to initial conditions, especially to greater sized micrograzers such as nauplii that could occur in large (20 l) microcosms. In fact, some copepods were observed in one of the microcosms (treatment LC LN LL replicate b) when large sample volumes were filtered at the end of the experiment (L. Yebra pers. comm.).

It is well known that upwelling leads to nutrient input and phytoplankton blooms that flatten the slopes in linear SAS (Reul et al. 2005, Rodríguez et al. 1998). This is usually explained by higher growth rates of diatoms (microphytoplankton) under nutrient-rich conditions (Malone 1980) and positive (ascending) vertical velocities (Rodríguez et al. 2001), whereas picophytoplankton remains unchanged. In our enclosure experiments, microphytoplankton increased and picophytoplankton decreased. A similar pattern was described by Reul et al. (2008) in upwelled nutrient-rich water in the northwestern part of the Strait of Gibraltar, where SAS became flatter due to both increasing nanophytoplankton and decreasing picophytoplankton abundance, especially *Synechococcus* and *Prochlorococcus*.

It is unlikely that under our experimental conditions (22.2 ± 1.8°C), *Synechococcus* was temperature- (Murphy & Haugen 1985) or nutrient-limited (Agawin 2000a,b). Consequently, the observed decrease in the abundance of *Synechococcus* and *Prochlorococcus* during the present experiment might be due to micrograzing by nanoflagellates (Tsai et al. 2007, 2009) and ciliates (Christaki et al. 1999). The fact that no significant relationship was found between *Synechococcus* abundance and their potential grazer could indicate additional factors that lowered the *Synechococus* abundance. A negative relationship between total diatom concentration and prokaryotic picophytoplankton abundance was observed for *Synechococcus*, but not for *Prochlorococcus* (Fig. 8), suggesting allelopathy as a possible co-factor that should be investigated in the future. Allelopathy can explain the coexistence of phytoplankton (Sarkar et al. 2006), species succession (Legrand et al. 2003) and size structure if donor and target species have different sizes (Granéli & Hansen 2006). In addition, lysis by virus and bacteria as well as fungal infection are other factors that affect the community structure and its size distribution, especially at the end of phytoplankton blooms (Brussaard et al. 2013). Thus, apart from silicate limitation (Neale et al. 2014), the cessation of diatoms at Day 6 (especially in the HC HN HL treatments) could also be due to other factors.

Temporal pattern

The overall temporal pattern in microcosms can be summarized in 4 stages:

(1) Initial acclimation and response to treatments (between Days −1 and 2): similar abundances of phytoplankton <15 µm, while biovolumes increased between Days 0 and 2. The SAS revealed increased abundances of cells >6 µm ESD, while ultraphytoplankton abundances remained similar.

(2) Grazing effects (Day 3): increased ciliate abundance indicated greater grazing capacity of microzooplankton that might be responsible for the significant decrease of ultraphytoplankton on Day 3.

(3) Nano–microphytoplankton diatom bloom (between Days 3 and 5): increasing diatom chl *a* concentrations in the nano- and, especially, microphytoplankton size-range depict a diatom bloom of cells that escaped micrograzing and were released from top-down control by mesozooplankton. This bloom was dominated by 2 diatoms species: *Leptocylindrus danicus* and *Chaetoceros* sp.

(4) Post-bloom conditions (HL treatments on Day 6): succession of the diatom bloom in the HL treatments on Day 6 reached post-bloom conditions, while growth in the LL treatment still continued.

Carbon, nutrient and light effects

Although the principal factor that affected the phytoplankton composition and SAS in the enclosures was a cascade effect caused by the removal of mesozooplankton, some differences between the treatments were detectable. The ANOVA indicated that high CO_2 concentrations and nutrient availability, and the interactions between CO_2 and nutrients and CO_2 and light significantly enhanced the growth of diatoms >20 µm. Increasing nutrient availability simulated the effects of fertilization of the euphotic layer, as expected for future scenarios of global climate change in coastal waters due to changing land use (Duce et al. 2008). In addition, increasing CO_2 concentrations and shifts in the light environment are expected worldwide in surface waters. The results of our study suggest that diatoms >20 µm should benefit from a global change-linked increase of CO_2 and nutrient availability in Mediterranean coastal area. The interactions with time are due to the different responses of the planktonic community to the treatments as succession progresses through the temporal pattern described previously. Note that changes in these temporal patterns due to global change could affect the temporal coupling in the food web.

Although the increased microphytoplankton concentration in the microcosm agreed with field studies in areas with fertilizing processes close to the sampling area, the Strait of Gibraltar (Gómez et al. 2000, Echevarría et al. 2002, Macias et al. 2006) and the upwelling area of the NW Alboran Sea (Ramírez et al. 2005, Reul et al. 2005, Mercado et al. 2012), the shape of the SAS and the magnitude of increasing microphytoplankton were not representative of field conditions. Apart from the mentioned cascade effects, settling is also an important factor that shapes SAS. According to size-dependent growth–loss rate balance spectra (Reul et al. 2006), cells >30 µm ESD would settle out of the enclosure assuming a 1 m mixing layer depth, and cells >141 µm would settle out from a 10 m mixing layer depth. Thus, according to the near surface stratifications at 2 m depth and a second stratification at 8 m at the sampling site (Neale et al. 2014), these cells would settle out of the surface stratified layer and dampen the diatom bloom that occurred in the enclosures.

Considering the response of primary producers to elevated CO_2, a positive effect on growth is the prevailing result in the literature, but neutral and negative effects have also been described (Gao et al. 2012 and references therein). Thus, the increasing diatom concentration in the HC treatments in our study agreed with the most frequently observed responses in phytoplankton. However, synergistic effects such as increasing stratification (which limits nutrient availability offshore) and simultaneously increasing CO_2 availability (which enhance growth) complicate predictions at a global scale (Gao et al. 2012), which become even more complicated when biotic factors are included.

Trimborn et al. (2013) described significant increases in the growth of *Chaetoceros debilis* under high CO_2 conditions in Antarctic waters, but also mentioned possible allelopathic effects of high *Pseudonitzschia subcurvata* abundance on *C. debilis* during competition experiments. Thus, while microcosm experiments permit the measurement of physiological parameters of plankton assemblages to different environmental drivers (CO_2, nutrients and light), caution is advisable in extrapolating the experimental results to the natural environment in terms of composition and size structure.

CONCLUSIONS

Microcosm experiments on natural assemblages are necessary to simulate possible future scenarios of

global climate change and the response of planktonic communities. However, they are more suitable for measurements on physiological responses of the surviving plankton assemblages to different environmental factors (CO_2, nutrients and light) than for predicting community composition and size structure, especially if the experiments last for more than 48 h.

While numerous field studies focus on physical (vertical velocities, density gradients, settling velocities) and bottom-up (nutrient availability) control of the phytoplankton SAS, this experiment points to the top-down control on SAS as an important factor in shaping phytoplankton size structure. This should therefore be included in SAS models and field studies. The complete SAS analysis revealed that enclosed communities still present a very complex system, and such systems are very sensitive to the initial conditions.

Acknowledgements. We thank the organizers and scientific committee for organizing the 9th GAP workshop in Málaga, Spain. We are extensively grateful for the financial contribution to the GAP-9 workshop 'Influence of the pulsed-supply of nitrogen on primary productivity in phytoplankton and marine macrophytes: an experimental approach', that included funds from Walz GmbH, several PAM fluorometers, Redox, University of Málaga General Foundation, Ministry of Economy and Competitivity of the Spanish Government (Acción Complementaria CTM2011-15659-E), and the Spanish Institute of Oceanography. The acquisition of the FlowCAM by the University of Málaga was co-financed by the 2008-2011 FEDER programme for scientific-technique infrastructure (Proposal number: UNMA08-1E005). We also thank L. Lubian from CSIC for providing cultures for flow cytometry calibration. BBE Moldanke supported the GAP workshop by providing the workstation, fingerprint and chl *a* calibration of the fluorospectrometer (FluoroProbe).

LITERATURE CITED

Agawin NSR, Duarte CM, Agustí S (2000a) Nutrient and temperature control of the contribution of picoplankton to phytoplankton biomass and production. Limnol Oceanogr 45:591–600

Agawin NSR, Duarte CM, Agustí S (2000b) Response of Mediterranean *Synechococcus* growth and loss rates to experimental nutrient inputs. Mar Ecol Prog Ser 206: 97–106

Álvarez E, López-Urrutia A, Nogueira E (2012) Improvement of plankton biovolume estimates derived from image-based automatic sampling devices: application to FlowCAM. J Plankton Res 34:454–469

Álvarez E, Moyano M, López-Urrutia A, Nogueira E, Scharek R (2014) Routine determination of plankton community composition and size structure: a comparison between FlowCAM and light microscopy. J Plankton Res 36:170–184

Bautista B, Harris RP (1992) Copepod gut contents, ingestion rates and grazing impact on phytoplankton in relation with the size structure of zooplankton and phytoplankton during a spring bloom. Mar Ecol Prog Ser 82:41–50

Behrenfeld MJ, O'Malley RT, Siegel DA, McClain CR and others (2006) Climate-driven trends in contemporary ocean productivity. Nature 444:752–755

Beutler M, Wiltshire KH, Meyer B, Moldaenke C and others (2002) A fluorometric method for the differentiation of algal populations *in vivo* and *in situ*. Photosynth Res 72: 39–53

Blanco JM, Echevarría F, García CM (1994) Dealing with size-spectra: some conceptual and mathematical problems. Sci Mar 58:17–29

Boyd PW, Doney SC (2002) Modelling regional responses by marine pelagic ecosystems to global climate change. Geophys Res Lett 29:53-1–53-4

Boyd PW, Jickells T, Law CS, Blain S and others (2007) Mesoscale iron enrichment experiments 1993–2005: synthesis and future directions. Science 315:612–617

Boyd PW, Strzepek R, Fu F, Hutchins DA (2010) Environmental control of open-ocean phytoplankton groups: now and in the future. Limnol Oceanogr 55:1353–1376

Brussaard CPD, Noordeloos AAM, Witte H, Collenteur MCJ, Schulz K, Ludwig A, Riebesell U (2013) Arctic microbial community dynamics influenced by elevated CO_2 levels. Biogeosciences 10:719–731

Calbet A (2001) Mesozooplankton grazing effect on primary production: a global comparative analysis in marine ecosystems. Limnol Oceanogr 46:1824–1830

Calbet A, Landry MR (1999) Mesozooplankton influences on the microbial food web: direct and indirect trophic interactions in the oligotrophic open ocean. Limnol Oceanogr 44:1370–1380

Calbet A, Saiz E (2013) Effects of trophic cascades in dilution grazing experiments: from artificial saturated feeding responses to positive slopes. J Plankton Res 35:1183–1191

Calbet A, Martínez AR, Isari S, Zervoudaki S and others (2012) Effects of light availability on mixotrophy and microzooplankton grazing in an oligotrophic plankton food web: evidences from a mesocosm study in Eastern Mediterranean waters. J Exp Mar Biol Ecol 424–425: 66–77

Christaki U, Jacques S, Dolan JR, Vaulot D, Rassoulzadegan F (1999) Growth and grazing on *Prochlorococcus* and *Synechococcus* by two marine ciliates. Limnol Oceanogr 44:52–61

Cury P, Shannon L, Shin YJ (2003) The functioning of marine ecosystems: a fisheries perspective. In: Sinclair M, Valdimarsson G (eds) Responsible fisheries in the marine ecosystem. FAO, Rome, p 103–123

Duce RA, LaRoche J, Altieri K, Arrigo KR and others (2008) Impacts of atmospheric anthropogenic nitrogen on the open ocean. Science 320:893–897

Echevarría F, García Lafuente J, Bruno M, Gorsky G and others (2002) Physical–biological coupling in the Strait of Gibraltar. Deep-Sea Res II 49:4115–4130

Essington T (2010) Trophic cascades in open ocean systems. In: Terborg J, Estes AJ (eds) Trophic cascades: predators, prey, and the changing dynamics of nature. Island Press, Washington, DC, p 91–105

Falkowski P, Scholes RJ, Boyle E, Canadell J and others (2000) The global carbon cycle: a test of our knowledge of Earth as a system. Science 290:291–296

Feely RA, Sabine CL, Lee K, Berelson W, Kleypas J, Favry VJ, Millero FJ (2004) Impact of anthropogenic CO_2 on the $CaCO_3$ system in the oceans. Science 305:362–366

Feng R, Weiming W, Zhenqing L (2009) Spatiotemporal complexity of a predator–prey system with the effect of noise and external forcing. Chaos Solitons Fractals 41: 1634–1644 05

Fessenden L, Cowles TJ (1994) Copepod predation on phagotrophic ciliates in Oregon coastal waters. Mar Ecol Prog Ser 107:103–111

Finkel ZV (2001) Light absorption and size scaling of light-limited metabolism in marine diatoms. Limnol Oceanogr 46:86–94

Gao K, Xu J, Gao G, Li Y and others (2012) Rising CO_2 and increased light exposure synergistically reduce marine primary productivity. Nat Clim Change 2:519–523

Gómez F, Echevarría F, García CM, Prieto L and others (2000) Microplankton distribution in the Strait of Gibraltar: coupling between organisms and hydrodynamic structures. J Plankton Res 22:603–617

Granéli E, Hansen PJ (2006) Allelopathy in harmful algae: A mechanism to compete for resources? In: Granéli E, Turner JT (eds) Ecology of harmful algae. Springer, Berlin, p 189–201

Hairston NG Jr, Hairston NG Sr (1993) Cause-effect relationships in energy flow, trophic structure, and interspecific interactions. Am Nat 142:379–411

Halvorsen E, Hirst AG, Batten SD, Tande KS, Lampit RS (2001) Diet and community grazing by copepods in an upwelled filament off the NW coast of Spain. Prog Oceanogr 51:399–421

Hare CE, Leblanc K, DiTullio GR, Kudela RM and others (2007) Consequences of increased temperature and CO_2 for algal community structure in the Bering Sea. Mar Ecol Prog Ser 352:9–16

Hernández-León S (2009) Top-down effects and carbon flux in the ocean: a hypothesis. J Mar Syst 78:576–581

Hoffmann LJ, Peeken I, Lochte K (2008) Iron, silicate and light co-limitation of three Southern Ocean diatom species. Polar Biol 31:1067–1080

Hooker SB, Van Heukelem L, Thomas CS, Claustre H and others (2009) The third SeaWiFS HPLC analysis round-robin experiment (SeaHARRE-3). NASA tech memo no. 2009–215849, NASA Center for AeroSpace Information, Hanover, MD

Irigoien X, Flynn KJ, Harris RP (2005) Phytoplankton bloom: a loophole in the microzooplankton grazing impact. J Plankton Res 27:313–321

Irwin AJ, Finkel ZV, Schofield OME, Falkowski PG (2006) Scaling-up from nutrient physiology to the size-structure of phytoplankton communities. J Plankton Res 28:459–471

Leboulanger C, Bouvy M, Carré C, Cecchi P and others (2011) Comparison of the effects of two herbicides and an insecticide on tropical freshwater plankton in microcosms. Arch Environ Contam Toxicol 61:599–613

Legendre L, Le Fèvre J (1989) Hydrodynamical singularities as controls of recycled versus export production in oceans. In: Berger WH, Smetacek VS, Wefer G (eds) Productivity of the ocean: present and past. John Wiley & Sons, New York, NY, p 49–63

Legendre L, Goselin M, Hirche HJ, Kattinger G, Rosenberg G (1993) Environmental control and potential fate of size-fractionated phytoplankton production in the Greenland Sea (75° N). Mar Ecol Prog Ser 98:297–313

Legrand C, Rengefors K, Fistarol GO, Graneli E (2003) Allelopathy in phytoplankton: biochemical, ecological and evolutionary aspects. Phycologia 42:406–419

Liu D, Sunc J, Zouc J, Zhang J (2005) Phytoplankton succession during a red tide of *Skeletonema costatum* in Jiaozhou Bay of China. Mar Pollut Bull 50:91–94

Macias D, García CM, Navas FE, Vazquez-Lopez-Escobar A, Mejias MB (2006) Tidal induced variability of mixing processes on Camarinal Sill (Strait of Gibraltar): a pulsating event. J Mar Syst 60:177–192

Mackey MD, Higgins HW, Mackey DJ, Wright SW (1996) CHEMTAX—a program for estimating class abundances from chemical markers: application to HPLC measurements of phytoplankton. Mar Ecol Prog Ser 144:265–283

Malone TC (1980) Algal size. In: Morris I (ed) The physiological ecology of phytoplankton. Blackwell Scientific Publications, Oxford, p 133–463

Mercado JM, Cortes D, García A, Ramírez T (2007) Seasonal and inter-annual changes in the planktonic communities of the northwest Alboran Sea (Mediterranean Sea). Prog Oceanogr 74:273–293

Mercado JM, Cortés D, Ramírez T, Gómez F (2012) Decadal weakening of the wind-induced upwelling reduces the impact of nutrient pollution in the Bay of Málaga (western Mediterranean Sea). Hydrobiologia 680:91–107

Mercado JM, Sobrino C, Neale PJ, Segovia M and others (2014) Effects of CO_2, nutrients and light on coastal plankton. II. Metabolic rates. Aquat Biol 22:43–57

Modigh M, Franzè G (2009) Changes in phytoplankton and microzooplankton population grazing experiments at a Mediterranean coastal site. J Plankton Res 31:853–864

Murphy LS, Haugen EM (1985) The distribution and abundance of phototrophic ultraplankton in the North Atlantic. Limnol Oceanogr 30:47–58

Neale PJ, Sobrino C, Segovia M, Mercado JM and others (2014) Effects of CO_2, nutrients and light on coastal plankton. I. Physico-chemical conditions and biological responses. Aquat Biol 22:25–41

Ohman MD, Runge JA (1994) Sustained fecundity when phytoplankton resources are in short supply: omnivory by *Calanus finmarchicus* in the Gulf of St. Lawrence. Limnol Oceanogr 39:21–36

Ohman MD, Snyder RA (1991) Growth kinetics of the omnivorous oligotrich ciliate *Strombidium* sp. Limnol Oceanogr 36:922–935

Orr JC, Fabry VJ, Aumont O, Bopp L and others (2005) Anthropogenic ocean acidification over the twenty-first century and its impact on calcifying organisms. Nature 437:681–686

Polovina JJ, Howell EA, Abecassis M (2008) Ocean's least productive waters are expanding. Geophys Res Lett 35: L03618, doi:10.1029/2007GL031745

Ramírez T, Cortés D, Mercado JM, Vargas-Yañez M, Sebastián M, Liger E (2005) Seasonal dynamics of inorganic nutrients and phytoplankton biomass in the NW Alboran Sea. Estuar Coast Shelf Sci 65:654–670

Reul A, Vargas JM, Jiménez-Gómez F, Echevar ia F, García-Lafuente J, Rodrígue J (2002) Exchange of planktonic biomass through the Strait of Gibraltar in late summer conditions. Deep-Sea Res II 49:4131–4144

Reul A, Rodríguez V, Jiménez-Gómez F, Blanco JM and others (2005) Variability in the spatio-temporal distribution and size-structure of phytoplankton across an upwelling area in the NW-Alboran Sea (W-Mediterranean). Cont Shelf Res 25:589–608

Reul A, Rodríguez J, Blanco JM, Rees A, Burkill PH (2006) Control of microplankton size structure in contrasting water columns of the Celtic Sea. J Plankton Res 28:449–457

Reul A, Rodríguez J, Guerrero F, González N and others

(2008) Distribution and size biomass structure of nanophytoplankton in the Strait of Gibraltar. Aquat Microb Ecol 52:253–262

Riebesell U, Lee K, Nejstgaard JC (2010) Pelagic mesocosms. In: Riebesell U, Fabry V, Hansson L, Gattuso JP (eds) Guide to best practices for ocean acidification research and data reporting. Publications Office of the European Union, Luxembourg, p 95–112

Rodríguez J, Blanco JM, Jiménez-Gómez F, Echevarría F and others (1998) Patterns in the size structure of the phytoplankton community in the deep fluorescence maximum of the Alboran Sea (southwestern Mediterranean). Deep-Sea Res 45:1577–1593

Rodríguez J, Tintoré J, Allen JT, Blanco JM and others (2001) Mesoscale vertical motion and the size structure of phytoplankton in the ocean. Nature 410:360–363

Rodríguez J, Jiménez-Gómez F, Blanco JM, Figueroa FL (2002) Physical gradients and spatial variability of the size structure and composition of phytoplankton in the Gerlache Strait (Antarctica). Deep-Sea Res II 49:693–706

Ros M, Miracle MR (1984) Variación estacional del fitoplancton del mar menor y su relación con la de un punto próximo en el Mediterráneo. Limnetica 1:32–42

Sabine CL, Feely RA, Gruber N, Key RM and others (2004) The oceanic sink for anthropogenic CO_2. Science 305: 367–371

Sarkar RR, Petrovskii SV, Biswas M, Gupta A, Chattopadhyay J (2006) An ecological study of a marine plankton community based on the field data collected from Bay of Bengal. Ecol Modell 193:589–601

Sarthou G, Timmermans KR, Blain S, Tréguer P (2005) Growth physiology and fate of diatoms in the ocean: a review. J Sea Res 53:25–42

Schlüter L (1998) The influence of nutrient addition on growth rates of phytoplankton groups, and microzooplankton grazing rates in a mesocosm experiment. J Exp Mar Biol Ecol 228:53–71

Schmoker C, Hernández-León S, Calbet A (2013) Microzooplankton grazing in the oceans: impacts, data variability, gaps of knowledge, and future directions. J Plankton Res 35:691–706

Slaughter AM, Bollens SM, Rollwagen Bollens G (2006) Grazing impact of mesozooplankton in an upwelling region off northern California, 2000–2003. Deep-Sea Res II 53:3099–3115

Sobrino C, Neale PJ, Lubián LM (2005) Interaction of UV-radiation and inorganic carbon supply in the inhibition of photosynthesis: spectral and temporal responses of two microalgae with different carbon concentration mechanisms. Photochem Photobiol 81:384–393

Sobrino C, Ward ML, Neale PJ (2008) Acclimation to elevated carbon dioxide and ultraviolet radiation in the diatom *Thalassiosira pseudonana*: effects on growth, photosynthesis, and spectral sensitivity of photoinhibition. Limnol Oceanogr 53:494–505

Sobrino C, Neale PJ, Phillips-Kress JD, Moeller RE, Porter J (2009) Elevated CO_2 increases sensitivity to ultraviolet radiation in lacustrine phytoplankton assemblages. Limnol Oceanogr 54:2448–2459

Sobrino C, Segovia M, Neale PJ, Mercado JM and others (2014) Effects of CO_2, nutrients and light on coastal plankton. IV. Physiological responses. Aquat Biol 22: 77–93

Sommer U, Sommer F, Feuchtmayr H, Hansena T (2004) The influence of mesozooplankton on phytoplankton nutrient limitation: a mesocosm study with northeast Atlantic plankton. Protist 155:295–304

Souza CS, Mafalda, P Jr, Sallés S, Ramirez T and others (2005) Seasonal and spatial trends in the mesozooplankton community at pluriannual temporal series in the NW of the Alborán Sea, Spain. Rev Biol Mar Oceanogr 40:45–54

Stibor H, Vadstein O, Diehl S, Gelzleichter A and others (2004) Copepods act as a switch between alternative trophic cascades in marine pelagic food webs. Ecol Lett 7:321–328

Sun J, Feng Y, Wang D, Song S, Jiang Y, Ding C, Wu Y (2013) Bottom-up control of phytoplankton growth in spring blooms in Central Yellow Sea, China. Deep-Sea Res II 97:61–71

Tomas CR (1997) Identifying marine phytoplankton. Academic Press, London

Tortell PD, DiTullio GR, Sigman DM, Morel FMM (2002) CO_2 effects on taxonomic composition and nutrient utilization in an Equatorial Pacific phytoplankton assemblage. Mar Ecol Prog Ser 236:37–43

Tortell PD, Payne CD, Gueguen C, Strzepek RF, Boyd PW, Rost B (2008) Inorganic carbon uptake by Southern Ocean phytoplankton. Limnol Oceanogr 53:1266–1278

Trimborn S, Brenneis T, Sweet E, Rost B (2013) Sensitivity of Antarctic phytoplankton species to ocean acidification: growth, carbon acquisition, and species interaction. Limnol Oceanogr 58:997–1007

Tsai AY, Chiang KP, Chan YF, Lin YC, Chang J (2007) PNF in the coastal western subtropical Pacific are important grazers on *Synechococcus* populations. J Plankton Res 29:71–77

Tsai AY, Chin WM, Chiang KP (2009) Diel patterns of grazing by pigmented nanoflagellates on *Synechococcus* spp. in the coastal ecosystem of subtropical western Pacific. Hydrobiologia 636:249–256

Utermöhl H (1958) Zur Vervollkommnung der quantitativen Phytoplankton-Methodik. Mitt Int Ver Theor Angew Limnol 9:1–38

van de Poll WH, Kulk G, Timmermans KR, Brussaard CPD and others (2013) Phytoplankton chlorophyll *a* biomass, composition, and productivity along a temperature and stratification gradient in the Northeast Atlantic Ocean. Biogeosciences 10:4227–4240

Volkmer B, Heinemann M (2011) Condition-dependent cell volume and concentration of *Escherichia coli* to facilitate data conversion for systems biology modelling. PLoS ONE 6:e23126

Appendix. (a) Example of the community aspect at the beginning of the experiment (seawater screened through 200 µm mesh) acquired with the FlowCAM at Day –1, and (b) example of the community aspect at the end of the experiment at Day 6 (replicate b of treatment HC HN LL)

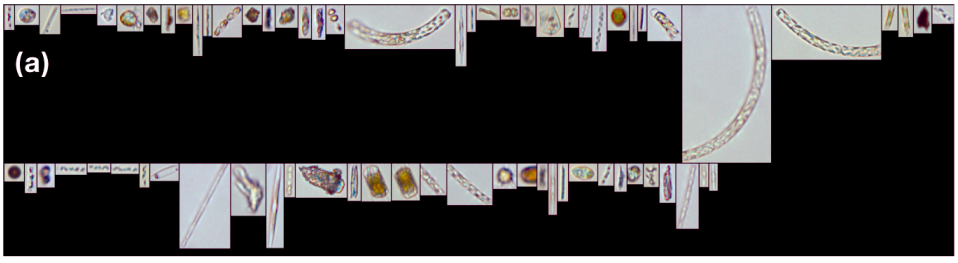

Submitted: December 19, 2013; Accepted: June 20, 2014 *Proofs received from author(s): August 20, 2014*